Conformational and Electronic Properties of the Two *Cis* (5*S*,6*R*) and (5*R*,6*S*) Diastereoisomers of 5,6-Dihydroxy-5,6-dihydrothymidine: X-ray and Theoretical Studies

Franck Jolibois,[†] Lucienne Voituriez,[†] André Grand,[‡] and Jean Cadet*,[†]

Département de Recherche Fondamentale sur la Matière Condensée/CEA/Grenoble, SESAM/LAN and SESAM/CC, 17, Rue des Martyrs, F-38054 Grenoble Cedex 09, France

Received July 21, 1995[⊗]

The structure of (+)-*cis*-(5*S*,6*R*)-5,6-dihydroxy-5,6-dihydrothymidine was obtained using X-ray crystallography [space group $P2_1$ with $a = 10.130(3)$ Å, $b = 6.434(9)$ Å, $c = 11.02(5)$Å, and $\beta = 112.646(2)°$]. The comparison of the two *cis* diastereoisomers of thymidine glycol (**I**, **II**) showed several structural and conformational differences. The solid state structures appear to be in agreement with the results of ^{1}H NMR studies which were carried out in aqueous solution. Conformational and electronic properties of the ground state of the molecules **I** and **II** were obtained using *ab initio* LSD-DFT theory. Only slight differences between the crystal structure and the optimized geometry are observed for each of the two oxidized nucleosides. On the other hand, molecules **I** and **II** exhibit significant differences in their electronic properties. In particular, the dipole moment of (5*S*,6*R*)-thymidine glycol (**I**) is twice smaller than that of the (5*R*,6*S*) diastereoisomer (**II**). It is noteworthy that these differences in the electronic properties between the two compounds may be related to changes in the rotameric population around the C4′−C5′ bond. The repartition of the electrostatic potential is different in the two compounds. These observations lead to a better understanding of the structural changes when the above lesions are included within a DNA molecule.

Introduction

Much attention has been devoted in the two past decades to the determination of the mechanisms of radical oxidation of nucleic acids associated with exposure to ionizing radiation (*1*−*5*). One of the major radiation-induced nucleobase lesions identified so far within naked (*6*−*10*) and cellular DNA (*11, 12*) is 5,6-dihydroxy-5,6-dihydrothymine. It is noteworthy that the so-called "thymine glycol" has been shown to be generated in cells under other oxidizing conditions including near-UV irradiation (*12*) treatment with hydrogen peroxide (*13*) and various carcinogens (*14, 15*). Efforts have also been made to gain insights into the biological role of 5,6-hydroxy-5,6-dihydrothymine (*16*). In this respect, the latter oxidized base does not appear to be a premutagenic lesion (*17*) when assessed in single-stranded DNA by using the transfection assay. It was also found that the coding properties of the diol were retained (*18*−*21*) despite the fact that the 5,6-ethylenic bond of the pyrimidine ring is saturated and the pyrimidine ring is no longer planar. Thymine glycol was found to be efficiently bypassed by the *Escherichia coli* Klenow fragment (*19, 22*). Similar observation was made in the same sequence context when single- and double-stranded genomes containing a thymine glycol residue were replicated in *E. coli* strains (*23*). However, since 5,6-dihydroxy-5,6-dihydrothymine was found to form an efficient hydrogen bond with adenine (*24*), it was concluded that this important class of oxidative DNA damage cannot be considered as an effective premutagenic lesion. It should be added that the presence of thymine glycol in pSV2 plasmids did not affect the transformation frequency in humans cells (*25*). Evidence was provided that the "thymine glycol" is a substrate for the *N*-glycosylase activity of *E. coli* endonuclease III (*26*−*29*). In addition, 5,6-dihydroxy-5,6-dihydrothymine was also found to be removed from oxidized DNA through an excision repair process mediated by the *E. coli* UV ABC nuclease complex (*30, 31*). Efforts were also made to determine the chemical and conformational features of 5,6-dihydroxy-5,6-dihydrothymine and related nucleoside derivatives. The absolute configuration of the four *cis* and *trans* diastereoisomers of 5,6-dihydroxy-5,6-dihydrothymidine which may be produced by the reaction of hydroxyl radicals (*5*) and through the photosensitized formation of a pyrimidine radical cation (*32*) was assigned (*33, 34*). The main change in the conformational properties of these four thymidine glycols, which was inferred from a detailed ^{1}H NMR study in aqueous solutions, deals with the shift in the dynamic equilibrium between the two puckered sugar conformers ^{2}E (C2′-*endo*) ↔ ^{3}E (C3′-*endo*) toward the ^{2}E form. This is more pronounced for the (6*S*) diastereoisomers (*35*). The presence of the thymine glycol in a duplex DNA was shown to induce significant distortion in the vicinity of the damage (*36*).

Relevant structural and conformational information regarding both the pyrimidine moiety and the furanose ring of the (−)-*cis*-(5*R*,6*S*)-"thymidine glycol" was inferred from a X-ray crystallographic investigation (*37*). In addition, it should be added that the X-ray structure of the *cis* isomer of 5,6-dihydrothymine was also resolved (*38*). Theoretical study of the structures of the four *cis* and *trans* enantiomers of 5,6-dihydroxy-5,6-dihydrothymine was carried out using Hartree−Fock *ab initio* quan-

* To whom correspondence should be addressed. Phone: (33)-76-88-49-87; Fax: (33)-76-88-50-90; E-Mail: cadet@drfmc.ceng.cea.fr.
[†] SESAM/LAN.
[‡] SESAM/CC.
[⊗] Abstract published in *Advance ACS Abstracts,* December 15, 1995.

0893-228x/96/2709-0298$12.00/0

tum chemical models (*39*). However, no theoretical investigations were made on the related nucleoside derivatives.

The aim of the present work is to provide structural and conformational information on the (+)-*cis*-(5*S*,6*R*)-"thymidine glycol" obtained by X-ray crystallographic diffraction and to compare the structure of the two *cis* diastereoisomers in the solid state. In addition, a theoretical study on both (+)-*cis*-(5*S*,6*R*) and (−)-*cis*-(5*R*,6*S*) diastereoisomers (**I**, **II**) was carried out using available crystallographic data. Emphasis was placed on the determination of conformational features of both the pyrimidine ring and the sugar moiety. This also allowed access to the electronic properties. The whole geometries of nucleosides were optimized with the local spin density (LSD) quantum chemical method. Electronic properties (partial charges, dipole moments, electrostatic potentials) were determined at the same level of calculation. We also determined dipole moments by using the *ab initio* Hartree−Fock theory.

Experimental Procedures

Chemicals. Thymidine, which was obtained from Sigma (St. Louis, MO), was used without further purification.

The (+)-*cis*-(5*S*,6*R*) and (−)-*cis*-(5*R*,6*S*) diastereoisomers of 5,6-dihydroxy-5,6-dihydrothymidine were prepared by the specific conversion of the (+)-*trans*-(5*R*,6*R*)- and (−)-*trans*-(5*S*,6*S*)-5-bromo-6-hydroxy-5,6-dihydrothymidine under slightly alkaline solutions. The (+)-*trans*-(5*R*,6*R*) and (−)-*trans*-(5*S*,6*S*) diastereoisomers of 5-bromo-6-hydroxy-5,6-dihydrothymidine were synthesized according to an adaptation of Baudish and Davidson procedure (*40*). Typically, 200 μL of bromine was added to 20 mL of water containing 2 g of thymidine (*41, 42*). The solution was kept in an ice bath for 15 min. Then, the excess of bromine was removed by bubbling nitrogen gas for 1 h. Subsequently, the aqueous solution was neutralized by adding 2.5 mL of 5 M sodium acetate. The solution was injected directly on a HPLC Prep LC/500 (Waters Associates, Milford, MA) apparatus, and the two thymidine bromohydrins were separated on a preparative (50 × 5 cm i.d.) octadecylsilyl silica gel column. The eluent was a mixture of water−methanol (80:20) at a flow rate of 100 mL/min. Evaporation to dryness of the fastest eluting HPLC fraction ($k' = 1.60$) gave 605 mg of the (5*S*,6*S*)-bromohydrin. The second HPLC eluting fractions ($k' = 2.64$) were combined and evaporated to dryness, yielding 1.450 g of the (5*R*,6*R*)-bromohydrin. Each of the two bromohydrins was transferred in a round flask. Then, 350 mL of water containing 350 mg of NH_4HCO_3 (for 1 g of bromhydrin) was added, and the resulting solution was heated for 3 h at 100 °C. The solutions were then evaporated and deposited on the above preparative column. The separation was achieved using water as the isocratic eluent at a flow rate of 100 mL/min. The (+)-(5*R*,6*R*)-bromohydrin leads to the formation of the *trans*-(−)- and *cis*-(+)-thymidine glycol. Evaporation to dryness in vacuum of the HPLC fraction ($k' = 3.61$) yields 620 mg of (+)-*cis*-(5*S*,6*R*)-5,6-dihydroxy-5,6-dihydrothymidine. The conversion of (−)-(5*S*,6*S*)-bromohydrin gives rise to the *trans*-(+)- and *cis*-(−)-thymidine glycol. Evaporation to dryness under reduced pressure of the HPLC fraction ($k' = 3.45$) gives 605 mg of (−)-*cis*-(5*R*,6*S*)-5,6-dihydroxy-5,6-dihydrothymidine. The four products were characterized by extensive spectroscopic measurements including FAB−mass spectrometry, U.V, circular dichroism, homonuclear ^{1}H NMR 1-D and 2-D COSY, 2-D NOESY, and heteronuclear ^{1}H−^{13}C analysis.

X-ray Structure Determination. (+)-*cis*-(5*S*,6*R*)-5,6-Dihydroxy-5,6-dihydrothymidine (**I**) was crystallized by evaporation from a concentrated water solution. The monoclinic $P2_1$ ($Z = 2$) space group with the following cell dimensions: $a = 10.130(3)$ Å, $b = 6.434(9)$ Å, $c = 11.02(5)$Å, and $\beta = 112.646(2)°$ were determined on a single crystal (approximately 0.2 × 0.2 × 0.25 mm) using an automatic ENRAF-NONIUS CAD4 diffractometer with Mo Kα (Ge monochromatized) radiation, by least-squares refinement of the setting angles for 25 reflections ($2\theta > 20°$). The data collection was performed on the same crystal, and intensities of 1309 independent reflections were collected in an ω scan mode (scan rate = 1 deg·min^{-1}). They were corrected for Lorentz and polarization factors but not for absorption. The stability of the crystal was monitored by measuring the intensities of three controlled reflections after every 100 measurements and 3600 s of exposure time. No significant trend in the intensities was observed during the data acquisition. Crystal data, together with details of the diffraction experiment and subsequent calculations, are listed in Table 1.

Table 1. Crystallographic Data and Refinement Parameters of I

formula	$C_{10}H_{16}N_2O_7$
space group	$P2_1$
a (Å)	10.130(3)
b (Å)	6.434(9)
c (Å)	11.020(5)
β (deg)	112.646(2)
cell volume (Å^3)	661.93
Z (molecules/cell)	2
density ρ (g·cm^{-3})	1.35
radiation	Mo Kα (Ge monochromatized)
diffractometer	ENRAF−NONIUS CAD4
scan range	$2° < 2\theta < 60°$
scan mode	ω scan (scan rate = 1deg·min^{-1})
data collected	$\pm h, +k, +l$
no. of data collected	1309
no. of parameters for mean square	180 using 759 reflections
R and R_w (%)	4.5 and 3.9

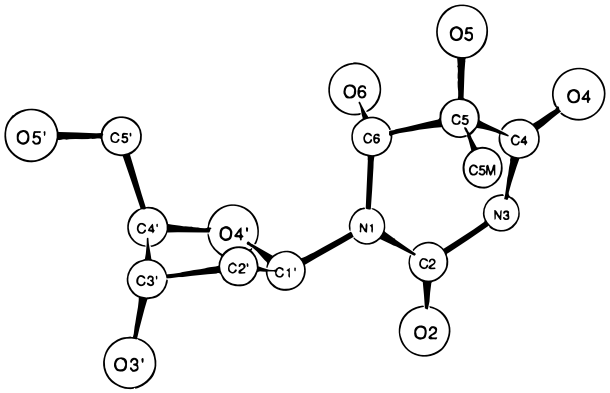

Figure 1. General structure of (+)-*cis*-(5*S*,6*R*)-5,6-dihydroxy-5,6-dihydrothymidine (**I**).

The structure was solved by direct methods using the MULTAN program (*43*). An *E*-map based on 190 phased reflections with $E > 1.6$ revealed the positions of all non-hydrogen atoms. The structure was refined by a least-squares method based on 759 reflections with $|F_o| > 2.6\sigma(F_o)$, using the XFLSN program (*44*). The positions of all hydrogen atoms were determined from a Fourier difference map and were fixed for refinement. Non-hydrogen atoms were assigned with anisotropic temperature factors whereas the hydrogens were assumed to have isotropic thermal motions ($B = 5$ Å^2). The final refinement of 180 variables reached values $R = 0.045$ and $R_w = 0.039$ respectively (with R defined by $\sum(|F_o| - |F_c|)/\sum|F_o|$ and R_w by $(\sum\omega(|F_o| - |F_c|)^2/\sum\omega|F_o|^2)^{1/2}$).

Structural and conformational data, which were obtained from the X-ray structure, are reported in Table S1 (non-hydrogen atom coordinates), Table S2 (hydrogen atom coordinates), Table S3 (bond lengths), Table S4 (bond angles), Table S5 (torsional angles), Table 2 (Cremer−Pople parameters for the pyrimidine ring (*45*)), Table 3 (hydrogen bonds), and Table 4 (pucker parameters for the sugar ring). Tables S1−S5 are available in the supporting information. The general structure of the (+)-*cis*-(5*S*,6*R*) diastereoisomer of 5,6-dihydroxy-5,6-dihydrothymidine (**I**) is shown in Figure 1, and a view of the packing is given in Figure 2.

Theoretical Calculations. The theoretical study of the conformational and electronic properties of both (+)-*cis*-(5*S*,6*R*)

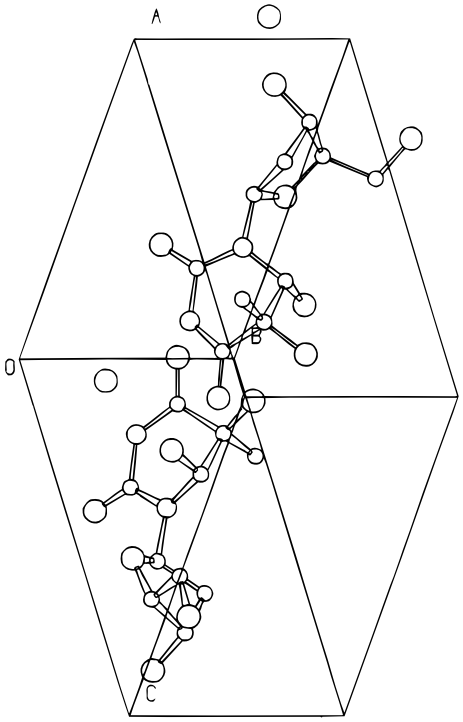

Figure 2. View of the packing of (+)-*cis*-(5*S*,6*R*)-5,6-dihydroxy-5,6-dihydrothymidine (**I**).

and (−)-*cis*-(5*R*,6*S*) diastereoisomers of 5,6-dihydroxy-5,6-dihydrothymidine (**I**, **II**) was carried out using crystallographic data (*37*). The approach involved a quantum chemistry *ab initio* method: the all-electron local spin version of density functional theory (LSD−DFT) (*46*, *47*).

Gaussian type orbital approach implemented in the Dgauss program (*48*, *49*) of UNICHEM 2.3 package (*50*) was used to solve LSD−DFT equations. An orbital basis set was required to describe molecular orbitals as well as an auxilliary one for the electronic distribution. The auxilliary basis set was also utilized to describe the exchange-correlation potential and energy. The double zeta valence plus polarization (DZVP) (621/41/1) orbitals basis set and the A1 auxilliary (7/3/3; 7/3/3) basis set (*51*, *52*) were used for this purpose. Nonlocal Becke Perdew (*53*−*55*) corrections to exchange and correlation energy were included after the SCF process, in a perturbation mode. This approach is communly used for such studies. As preliminary attempts, several calculations were carried out using different methods (DFT, Hartree−Fock, semiempirical) and several basis sets for the DFT method (DZVP, DZVP2, TZVP). It appears that the DFT method with DZVP plus A1 basis sets is the more appropriate for the present study.

Ground state geometries were obtained using the gradient optimization technique (*56*) and were used for the determination of electronic properties. The electronic features determined are the following:

- Mulliken charge population analysis (*57*);
- Dipole moment, according to the equation:

$$\mu_m = \sum_A Z_A \mu^m(A) - \int \varrho(r) \mu^m(r)\, dr$$

where μ^m is defined with regard to the center of mass A as:

$$\mu^m = \mu^{mx,my,mz} = (x - Ax)^{mx}(y - A_y)^{my}(z - A_z)^{mz}$$

- Electrostatic potential as defined by:

$$V_{esp}(r) = \sum_A Z_A / |R_A - r| - \int \varrho(r)/|r - r'| dr'$$

The determination of dipole moment and electrostatic potential was based on the electronic density obtained from molecular orbitals. All properties were calculated on a CRAY 94 supercomputer with 4 CPU process (CEA-CEN, Grenoble).

Results and Discussion

(a) Crystal Structure of (+)-*cis*-(5*S*,6*R*)-5,6-Dihydroxy-5,6-dihydrothymidine. (1) Pyrimidine Ring. Bond lengths and bond angles are given in Tables S3 and S4, respectively. The pyrimidine ring exhibits a half-chair conformation geometry as already described for 5,6-saturated 2,4-dioxopyrimidine derivatives (*37*, *38*, *58*). The best four-atom mean plane is defined by N1, C2, N3, and C4 atoms. The average displacement of the related atoms from the mean plane is 0.02 Å. On the other hand, the C5 and C6 atoms are displaced 0.40 Å to the right and 0.39 Å to the left, respectively (see Figure 3). When the base is viewed in its *anti* conformation with respect to the *N*-glycosyl bond, the left represents displacement toward O4′ and the right toward C2′. On the other hand, for the (5*R*,6*S*) diastereoisomer (**II**), the C5 and C6 atoms are displaced to the left and the right, respectively (*37*), as expected from the enantiomeric relationship existing between the two pyrimidine bases of **I** and **II**. The 5-methyl and the 6-hydroxyl groups of both **I** and **II** adopt a pseudoaxial orientation, whereas the 5-hydroxyl group is pseudoequatorial. Similar structural features were also inferred from the X-ray crystallographic structure (*38*) and the *ab initio* calculations (*39*) of *cis*-thymine glycol. It should be added that the substituents on the C5−C6 carbons of **I** are orientated in the range of classically-staggered saturation system (±60°,180°) (see Table S5).

Cremer−Pople data for **I** and **II** are reported in Table 2. **I** appears in the "Southern" CP hemisphere S(CP) (90° < θ < 180°), whereas **II** is in the "Northern" CP hemisphere N(CP) (0° < θ < 90°). **I** shows the most pronounced extent of puckering ($Q_{\mathbf{I}} = 0.52$ Å, $Q_{\mathbf{II}} = 0.48$ Å) with a $\phi_{\mathbf{I}}$ value = 89°, which is different from that of **II** ($\phi_{\mathbf{II}} = 272°$). This is in agreement with the predictions of Hruska *et al.* (*37*).

(2) N-Glycosyl Bond. The N1−C1′ bond length (Table S3) and the bond angles involving N1−C1′ (Table S4) are similar to those of **II**. By considering χ(O4′−C1′−N1−C2) and χ'(O4′−C1′−N1−C6) torsional angles (Table S5), **I** adopts an *anti* conformation about the *N*-glycosyl bond. However, we may note slight differences in the values of χ (−96.9° and −111.6° for **I** and **II**, respectively) and χ' (62.1° and 67.6° for **I** and **II**, respectively). These are related to the differences in the pucker of the pyrimidine bases (the base of **I** is in the S(CP) hemisphere, whereas the base of **II** is in the N(CP) hemisphere). The latter data clearly indicate that the H6 atom of **I,** which adopts a pseudoequatorial orientation, is located on the right side of the pyrimidine ring.

(3) Sugar Moiety. The respective bond lengths and bond angles regarding the sugar moiety of **I** and **II** are similar. The furanose ring of **I** adopts a C2′-*endo* conformation with a phase angle of pseudorotation P = 169.9° (*S* type pucker $^2T_3$ (*59*)) and a maximum amplitude of pucker $\tau_m = 37.4°$ (Table 4). The *S* (C2′-*endo*) type of pucker of **I** is more pronounced than that of **I** ($P = 151.2°$, $\tau_m = 36.5°$).

The staggered orientation of the exocyclic hydroxymethyl group about the C4′−C5′ bond of thymidine glycol **I** is *trans* with $\gamma = -71.8°$ (*60*). Comparison between the crystallographic data of **I** and **II** shows important differences in the C4′−C5′ bond geometry since **II** exhibits a *gauche*$^+$ conformation. Interestingly, the solid state

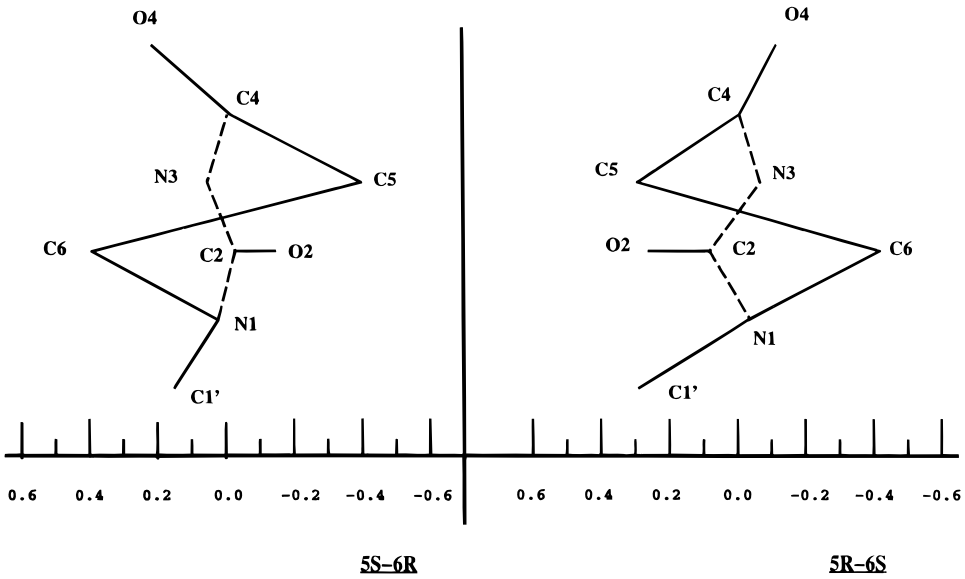

Figure 3. Schematic view of the base of the two diastereoisomers **I** and **II**. The horizontal axis gives the deviation in Å to the left (positive) and to the right (negative) of the best four-atom mean plane, N1−C2−N3−C4.

Table 2. Cremer−Pople Puckering Parameters for Pyrimidine Bases

molecule[a]	Q (Å)	θ (deg)	ϕ (deg)
1	0.52	124	89
2	0.46	129	96
3	0.48	62	272
4	0.50	59	268

[a] (1) (5*S*,6*R*) crystal structure; (2) (5*S*,6*R*) optimized geometry; (3) (5*R*,6*S*) crystal structure; (4) (5*R*,6*S*) optimized geometry.

conformational features of **I** are in agreement with the preferential *trans* conformation of the 5-(hydroxymethyl) group in aqueous solution as inferred from a ^{1}H NMR study (*35*).

(4) Hydrogen Bonds. Hydrogen bond data are listed in Table 3. Molecular packing is stabilized by three weak (distance D−A >2.8 Å) and one strong (distance D−A <2.8 Å) hydrogen bonds in the following network: N3−H...O5−H...O4′−H...O6−H...O5. Three other strong hydrogen bonds are involved with a water solvent molecule: These include O3′−H...O10, O10−H1...O4′, and O10−H2...O3′. Finally, an intermolecular close contact is noted between H6 and O2 (2.24 Å). The O5, O4′, and O6 donor atoms also serve as acceptors, but this is not the case for the O3′ and N3 atoms. Because of molecular configuration differences, hydrogen bonds are not identical for the two compounds **I** and **II**. The O2 atom, which participates in a weak bond in the (5*R*,6*S*) diastereoisomer **II** (*37*), is involved in a close contact in the (5*S*,6*R*) diastereoisomer **I**. We also established that the H6 atom of **I** is included in an intermolecular close contact with O2, whereas the related atom of **II** participates in an intramolecular close contact with O5′. It should be added that, in both cases, O4 does not participate in molecular packing.

(b) Theoretical Conformational Properties. A geometry optimization of the two *cis* (5*S*,6*R*) and (5*R*,6*S*) diastereoisomers of 5,6-dihydroxy-5,6-dihydrothymidine (**I**, **II**) was carried out using the local spin density theory with the X-ray coordinates as starting data. It should be noted that the optimized geometries of the molecular structures were obtained in empty space at 0 K. The geometry optimization was carried out on the whole structure, without any constraints. It has to be added that the calculations were based on the gradient optimization technique, using Cartesian coordinate representation.

(1) Pyrimidine Ring. The respective bond lengths and bond angles of the crystals and optimized structures are similar (Tables S3 and S4). Comparison between dihedral angles (Table S5) shows that the conformational features are identical for all geometries. These include a pseudo-half-chair conformation for the pyrimidine ring, a pseudoaxial orientation for the 5-methyl and 6-hydroxyl groups, and a pseudoequatorial conformation for the 5-hydroxyl group. Considering the Cremer−Pople data (Table 2), geometries of **I** are in the "Southern" CP hemisphere with a more pronounced puckered conformation for the crystal structure ($Q_{\mathbf{I}} = 0.52$ Å and $Q_{\mathbf{I}\text{-LSD}} = 0.46$ Å). It should be noted that **I** represents the (5*S*,6*R*) crystal structure and **I**-LSD, the (5*S*,6*R*) calculated geometry. We used the same notation for the (5*R*,6*S*) diastereoisomer **II**, where **II**-LSD represents the calculated geometry. In contrast, geometries of **II** are in the "Northern" CP hemisphere with a more pronounced puckering for the optimized structure ($Q_{\mathbf{II}} = 0.48$ Å and $Q_{\mathbf{II}\text{-LSD}} = 0.50$ Å). The best contiguous four-atom plane is defined by N1, C2, N3, and C4 as for the X-ray structures. Displacement of C5 to the right is higher for

Table 3. Hydrogen Bonds and Close Contact for (5*S*,6*R*) Structure

D−H...A	acceptor A	D−H (Å)	H...A (Å)	D...A (Å)	D−H...A (deg)
O3′-H...O10	x, y, z	1.05	1.67	2.68	159.8
O10-H...O4′	$-x, -1/2 + y, 2 - z$	1.00	1.93	2.84	149.9
O10-H...O3′	$-x, 1/2 + y, 2 - z$	0.94	2.40	2.77	102.9
N3-H...O5	$x, -1 + y, z$	1.01	2.16	3.08	150.8
O5-H...O4′	$1 + x, y, z$	0.91	2.39	3.14	140.3
O4′-H...O6	$-x, 1/2 + y, 1 - z$	0.88	1.96	2.71	140.9
O6-H...O5	$1 - x, -1/2 + y, 1 - z$	0.95	2.44	3.31	151.4
C6-H...O2	$x, 1 + y, z$	1.11	2.24	3.19	140.3

Table 4. Pucker Parameters for Sugar Fragments[a]

	1	2	3	4
P (deg)	169.9	159.4	151.2	171.8
τ_m (deg)	37.4	37.8	36.5	35.4

[a] (1) (5*S*,6*R*) crystal structure; (2) (5*S*,6*R*) optimized geometry; (3) (5*R*,6*S*) crystal structure; (4) (5*R*,6*S*) optimized geometry.

the crystal structure of **I** (crystal: 0.40 Å, optimized: 0.28 Å). On the other hand, displacement of C6 to the left is more pronounced for the calculated geometry (crystal: 0.39 Å, optimized: 0.43 Å). It should be added that the displacement of C5 to the left for **II** is more pronounced in the theoretical geometry (crystal: 0.28 Å, optimized: 0.36 Å). In addition, displacement of C6 to the right is more important in the crystal structure (crystal: 0.42 Å, optimized: 0.38 Å).

(2) *N*-Glycosyl Bond. The respective N1−C1′ bond lengths and N1−C1′−X bond angles are similar (Tables S3 and S4) for the crystal structures and optimized geometries. The values of χ(O4′−C1′−N1−C2) torsion angles are indicative of an *anti* conformation about the *N*-glycosyl bond for the two *cis*-thymidine glycols (**I**, **II**), both in the solid state and from theoretical calculations. However, according to the displacement of C6 toward O′4 in the (5*S*,6*R*) diastereoisomer, χ'(O4′−C1′−N1−C6) is higher in the crystal structure than in the optimized geometry ($\chi'_{crystal}$: 62.1°, $\chi'_{optimized}$: 49.8°). For the (5*R*,6*S*) diastereoisomer **II**, χ' exhibits a higher value in the crystal structure ($\chi'_{crystal}$: 67.6°, $\chi'_{optimized}$: 66.9°), and the displacement of C6 toward C2′ is more important in the crystal.

(3) Sugar Moiety. All bond lengths and bond angles of the crystal and optimized structures of **I** and **II** are similar. The pucker parameters for the furanose ring of the four experimental and theoretical geometries are reported in Table 4. In all cases, the furanose ring adopts a C2′-*endo* conformation (151.2° ≤ P ≤ 171.8°). The data for the crystal structure of **II** and the optimized geometries of **I** are indicative of a $^2T_1$ *S* type pucker. The two others structures display a $^2T_3$ *S* type pucker. It should be noted that the *S* (C2′-*endo*) type of pucker for the (5*R*,6*S*) optimized structure exhibits the highest value of pseudorotation angle (P = 171.8°), whereas the (5*R*,6*S*) crystal structure shows the smallest value (P = 151.2°). Comparison of the two (5*S*,6*R*) geometries shows that the crystal structure (P = 169.9°) has a stronger S (C2′-*endo*) type of pucker than the optimized geometry (P = 159.4°). As already mentioned, the crystal structure of **I** has a stronger *S* (C2′-*endo*) puckered geometry than the crystal of **II**. Interestingly, a similar trend was noted for the corresponding optimized geometries. In addition, the differences in the puckering features of the two optimized structures are similar to that observed for the crystal structures.

Conformation about C4′−C5′ is *trans* for both experimental and theoretical geometries of **I**, whereas a *gauche*$^+$ orientation is noted for the two geometries of **II**. The differences between the crystal and optimized structures are close to 10°.

(c) Electronic Properties. From the results of geometry optimization, a study of the electronic properties was carried out in order to gain insight into molecular reactivity features. UNICHEM2.3 package allows the determination of some electronic properties based on the use of the LSD-DFT method. These include dipole moments, point charges, and electrostatic potential. As a first general observation, it is important to note that the inversion of the C6 and C5 configurations induces significant changes in the electronic properties.

Table 5. Dipole Moments (in D) of the Two Diastereoisomers I and II Calculated with Differents Methods and Basis Sets

	(5*S*,6*R*)	(5*R*,6*S*)
DFT	3.56	7.12
Hartree−Fock 3-21G	4.15	7.79
Hartree−Fock 3-21G**	4.13	7.67
Hartree−Fock 6-21G	4.09	7.71

(1) Point Charges and Dipole Moments. Point charges are given in Table S6 (available in the supporting information) and dipole moments are reported in Table 5 and Figure 4. Dipole moments μ are different in both value and direction. Surprisingly, the value of $\mu_{\mathbf{I}}$ (dipole moment of **I**) is twice smaller than the value of $\mu_{\mathbf{II}}$ (dipole moment of **II**). Other calculations of the dipole moment were carried out using the *ab initio* Hartree−Fock theory program GAUSSIAN 92 (*61*) with several basis sets (see Table 5). In each case, the values of $\mu_{\mathbf{I}}$ are approximatively twice smaller than those of $\mu_{\mathbf{II}}$. Therefore, it may be concluded that the observed difference in the values does not depend on either the method used or a basis set effect. In addition, the directions of the dipole moments are also different. Qualitatively, $\mu_{\mathbf{I}}$ and $\mu_{\mathbf{II}}$ directions are along the straight lines defined by (C1′,C2′) and (N3,-C5′), respectively.

Partial charges are similar for the related atoms, with the exception of C6, H6, and O5′ atoms. Partial charge on O5′ is higher for **I**, −0.497 C, than for **II**, −0.544 C. Point charge on H6 is higher for **I**, 0.328 C, than for **II**, 0.227 C.

At the present time, we can rationalize these differences in term of change in the electronic density. The calculation of these properties is directly connected to the electronic distribution. Differences in conformationnal features and, especially, the existence of an intramolecular close contact between O5′ and H6 in (5*R*,6*S*) diastereoisomer **II** induce important modifications in the electronic density. Effectively, the latter close contact is likely to lead to an electronic delocalization from H6 to O5′. This large delocalization provides an explanation for the observed differences in dipole moment and point charges between the two diastereoisomers. The close contact also leads to a decrease in the partial charge on C6 (for **II**: −0.258 C, for **I**: −0.126 C).

(2) Electrostatic Potential. The electrostatic potential at a point r is defined as an electrostatic interaction energy of a probe charge of value +1 au with all nuclei and electrons of the concerned molecular system. According to this definition, regions of negative electrostatic potential are favorable to electrophilic attack including hydrogen bonding.

Negative electrostatic potentials at −24 kcal/mol are observed for both compounds **I** and **II** as shown in Figure 5. Negative regions are localized around all the oxygen atoms with the exception of the O5′ atom for **II**, which is involved in close contact with H6. We can observe a decrease of the electrostatic potentials in the vicinity of the O4 and O5 atoms for **I** and near O3′ and O4′ for **II**. Each of the thymidine glycols **I** and **II** exhibits a region of high reactivity delocalized around a few different atoms. For the glycol **I**, the negative well is localized around O2, O6, and O4′, whereas the reactivity region is localized around O2, O4, O6, and O5 atoms for the glycol **II**.

As for the two other properties, the modifications of electrostatic potential can be rationalized in terms of

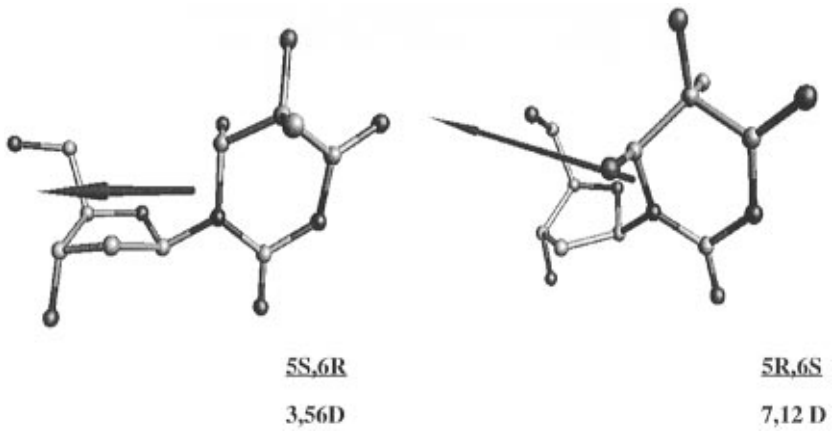

Figure 4. Representation of the dipole moment of the two diastereoisomers **I** and **II**.

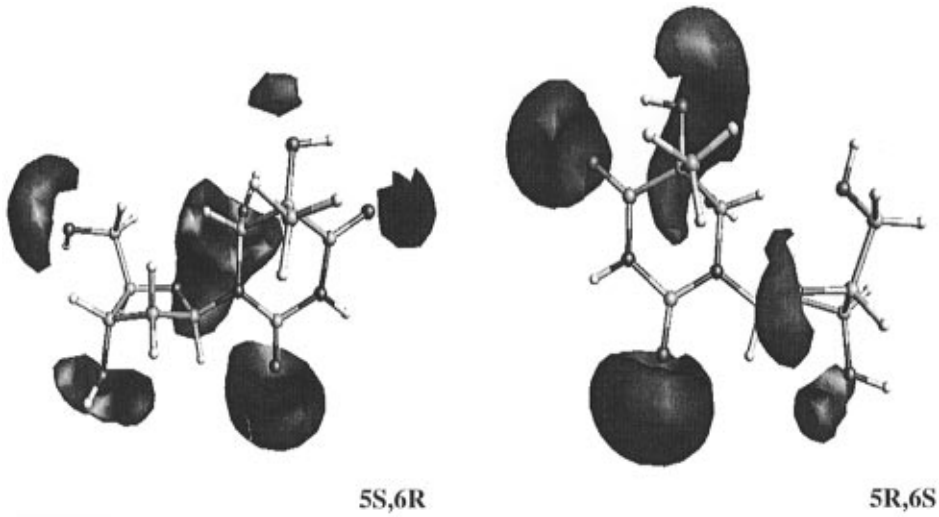

Figure 5. Volumetric representation of the electrostatic potential at −24 kcal/mol of the two diastereoisomers **I** and **II**.

electronic density delocalization. The observed decrease in the negative electrostatic potential region near O4 of **I** is likely to be associated with a reduction in reactivity around the latter atom including hydrogen bonding. This is reflected by molecular packing (see before) in which O4 is not implicated in any hydrogen bond. It should be noted that the atom is directly implicated in a hydrogen bond with adenine in the DNA double strand.

Conclusion

Both reported experimental and theoretical results show that the two *cis* diastereoisomers of thymidine glycol exhibit differences in the conformational and electronic properties. The structures of the two compounds are in agreement with the results of the ^{1}H NMR analysis in aqueous solution. The general conformation of the pyrimidine ring is similar to that was found for the *cis*-thymine glycol (*38, 39*). We may note that the presence of the sugar has little effect on the base conformation.

Important differences were observed in the electrostatic potential, the partial charges, and the dipole moment of the two compounds. The principal cause of these changes may be explained in term of an intramolecular close contact between H6 and O5′ atoms in the thymidine glycol **II** which does not exist in the other diastereoisomer **I**. This is due to differences in the rotameric population of the C4′−C5′ bond which is *trans* in the diastereoisomer **I** and *gauche*$^+$ in the diastereoisomer **II**. This close contact may lead to modifications in the electronic density repartition which consequently may give rise to differences in the electronic properties.

The presence of **I** and **II** within DNA may cause severe structural distortions of the double strand (*36, 39*). Yet, we can envisage a difference of behavior between the two *cis*-thymidine glycols. The differences in the electrostatic interactions within DNA are expected to be related to modifications in dipole moments and electrostatic potentials. It should be remembered that the dipole moment of the (5*R*,6*S*) diastereoisomer is twice that of the (5*S*,6*R*) diastereoisomer. Considering the repartition of the negative electrostatic potentials (Figure 5), again it is likely that the extend of the distortion of the DNA helix will depend on the stereoconfiguration of the thymidine glycol.

Acknowledgment. This research was partly supported by a grant from the French Ministry of Science and Research. We thank Prof. Robert Subra and Prof. Vincenzo Barone for fruitful discussions.

Supporting Information Available: Final atomic crystallographic coordinates of both non-hydrogen (Table S1) and hydrogen (Table S2) atoms of the (+)-*cis*-(5*S*,6*R*)-5,6-dihydroxy-5,6-dihydrothymidine, bond lengths (Table S3), bond angles (Table S4), torsion angles (Table S5), and the partial charges of the two *cis* diastereoisomers of the 5,6-dihydroxy-5,6-dihydrothymidine (Table S6) (9 pages). This material is contained in many libraries on microfiche, immediately follows this article in the microfilm version of the journal, can be ordered from the ACS, and can be downloaded from the Internet; see any current

masthead page for ordering information and Internet access instructions.

References

(1) Téoule, R., and Cadet, J. (1978) Radiation-induced degradation of the base component in DNA and related substances. Final products. In *Effects of Ionizing Radiation on DNA* (Hütterman, J., Köhnlein, W., Téoule, R., and Bertinchamps, A. J., Eds.) pp 171−203, Springer, Berlin.

(2) Téoule, R. (1987) Radiation-induced DNA damage and its repair. *Int. J. Radiat. Biol.* **51**, 573−589.

(3) von Sonntag, C. (1987) *The Chemical Basis of Radiation Biology*, Taylor and Francis.

(4) Teebor, G. W., Boorstein, R. J., and Cadet, J. (1988) The repairability of oxidative free radical mediated damage to DNA. *Int. J. Radiat. Biol.* **54**, 131−150.

(5) Cadet, J. (1994) DNA damage caused by oxidation, deamination, ultraviolet radiation and photoexcited psoralens. In *DNA adducts: Identifications and biological significance* (Hemminki, K., Dipple, A., Shuker, D. E. G., Kadlubar, F. F., Segerbäck, D., and Bartsch, H., Eds.) IARC Scientific Publications 125, pp 245−276, International Agency for Cancer Research, Lyon.

(6) Téoule, R., Bert, C., and Bonicel, A. (1977) Thymine fragment damage retained in the DNA polynucleotide chain after gamma irradiation in aerated solution. *Radiat. Res.* **72**, 190−200.

(7) Frenkel, K., Goldstein, M., and Teebor, G. W. (1981) Identification of the *cis*-thymine glycol moiety in chemically oxidized and γ irradiated deoxyribonucleic acid by high-pressure liquid chromatography analysis. *Biochemistry* **24**, 7566−7571.

(8) Hubbard, K., Huang, H., Laspia, M. F., Erlanger, B. F., and Wallace, S. S. (1989) Immunochemical quantitation of thymine glycol in oxidized and X-irradiated DNA. *Radiat. Res.* **118**, 257−268.

(9) Dizdaroglu, M. (1985) Application of capillary gas chromatography−mass spectrometry to chemical characterization of radiation-induced base damage of DNA: implications for assessing DNA repair processes. *Anal. Biochem.* **144**, 593−603.

(10) Teebor, G. W., Cummings, A, Frenkel, K., Shaw, A., Voituriez L., and Cadet J. (1987) Quantitative measurement of the diastereoisomers of *cis* thymidine glycol in γ-irradiated DNA. *Free. Radical Res. Commun.* **2**, 303−309.

(11) Hariharan, P. V., and Cerutti, P. A. (1972) Formation and repair of γ-ray induced thymine damage in *Micrococcus radiodurans*. *J. Mol. Biol.* **66**, 65−81.

(12) Hariharan, P. V., and Cerutti, P. A. (1976) Excision of ultraviolet and gamma ray products of the 5,6-dihydroxydihydrothymine type by nuclear preparations of xeroderma pigmentosum cells. *Biochim. Biophys. Acta* **447**, 375−378.

(13) Kaneko, M., Leadon, S. A., and Ito, K. (1988) Relationship between the induction of mitotic gene conversion and the formation of thymine glycols in yeast *S. cerivisiae* treated with hydrogen peroxyde. *Mutat. Res.* **207**, 17−22.

(14) Kaneko, M., and Leadon, S. A. (1986) Production of thymine glycols in DNA by N-hydroxy-2-naphthylamine as detected by a monoclonal antibody. *Cancer Res.* **46**, 71−73.

(15) Leadon, S. A. (1990) Production and repair of DNA damage in mammalian cells. *Health Phys.* **59**, 15−22.

(16) Cathchart, R., Schwiers, E., Saul, R. L., and Ames, B. N. (1984) Thymine glycol and thymidine glycol in human and rat urine: A possible assay for oxidative DNA damage. *Proc. Natl. Acad. Sci. U.S.A.*. **81**, 5633−5637.

(17) Hayes, R. C., Petrullo, L. A., Huang, H., Wallace, S. S., and Leclerc, J. E. (1988) Oxidative damage in DNA: lack of mutagenicity by thymine glycol lesions. *J. Mol. Biol.* **201**, 239−246.

(18) Ide, H., Kow, Y. W., and Wallace, S. S. (1985) Thymine gycol and urea residues in M13 DNA constitute replicative blocks *in vitro*. *Nucleic Acids Res.* **13**, 8035−8052.

(19) Hayes, R. C., and Leclerc, J. E. (1986) Sequence dependence for bypass of thymine glycols in DNA by DNA-polymerase I. *Nucleic Acids Res.* **14**, 1045−1061.

(20) Clark, J. M., and Beardsley, G. P. (1986) Thymine glycol lesions terminate chain elongation by DNA-polymerase I in vitro. *Nucleic Acids Res.* **14**, 737−749.

(21) Ide, H., and Wallace, S. S. (1988) Dihydrothymine and thymidine glycol triphosphates as substrates for DNA polymerases: differential recognition of thymine C5−C6 bond saturation and sequence specificity of incorporation. *Nucleic Acids Res.* **16**, 11339−11354.

(22) Evans, J., Maccabee, M., Hatahet, Z., Courcelle, J., Bockrath, R., Ide, H., and Wallace, S. S. (1993) Thymine ring saturation and fragmentation products: lesion bypass, misinsertion and implications for mutagenesis. *Mutat. Res.* **299**, 147−156.

(23) Basu, A. K., Loechler, E. L., Leadon, S. A., and Essigmann, J. M. (1989) Genetic effetcs of thymidine glycol: Site-specific mutagenesis and molecular modeling studies. *Proc. Natl. Acad. Sci. U.S.A.*. **86**, 7677−7681.

(24) Clark, J. M., and Beardsley, G. P. (1987) Functional effects of *cis*-thymine glycol lesions on DNA syntheses in vitro. *Biochemistry* **26**, 5398−5403.

(25) Spivak, G., Leadon, S. A., Vos, J. M., Meade, S., Hanawalt, P. C., and Ganesan, A. K. (1988) Enhanced transforming activity of pSV2 plasmids in human cells depends on the type of damage introduced into the plasmid. *Mutat. Res.* **193**, 97−108.

(26) Demple, B., and Linn, S. (1980) DNA-*N*-glycosylases and UV repair. *Nature* **287**, 203−208.

(27) Breimer, L. H., and Lindahl, T. (1985) Thymine lesions produced by ionizing radiation in double-stranded DNA. *Biochemistry* **24**, 4018−4022.

(28) Dizdaroglu, M., Laval, J., and Boiteux, S. (1993) Substrate specificity of the *Escherichia coli* Endonuclease III: Excision of thymine and cytosine-derived lesions in DNA produced by radiation-generated free radicals. *Biochemistry* **32**, 12105−12111.

(29) Cunningham, R. P., Ahern, H., Xing, D., Thayer, M. M., and Tainer, J. A. (1994) Structure and function of *Escherichia coli* Endonuclease III. *Ann. N.Y. Acad. Sci.* **726**, 215−222.

(30) Lin, J. J., and Sancar, A. (1989) A new mechanism for repairing oxidative damage to DNA: (A)BC exonuclease removes AP sites and thymine glycols from DNA. *Biochemistry* **28**, 7979−7984.

(31) Kow, Y. W., Wallace, S. S., and Van Houten, B. (1990) UvvABC nuclease complex repairs thymine glycol, an oxidative DNA base damage. *Mutat. Res.* **235**, 147−156.

(32) Decarroz, C., Wagner, J. R., van Lier, J. E., Murali Krishna, C., Riesz, P., and Cadet, J. (1986) Sensitized photo-oxidation of thymidine by 2-methyl-1,4-naphthoquinone. Characterization of the stable photoproducts. *Int. J. Radiat. Biol.* **50**, 491−505.

(33) Cadet, J., Ulrich, J., and Téoule, R. (1975) Isomerization and new specific synthesis of thymine glycol. *Tetrahedron* **31**, 2057−2061.

(34) Cadet, J., Ducolomb, R., and Téoule, R. (1977) Préparation, isomérisation et configuration absolue des "hydrates" de thymine (Preparation, isomerization, and absolute configuration of thymidine "hydrates"). *Tetrahedron* **33**, 1603−1607.

(35) Cadet, J., Ducolomb, R., and Hruska, F. E. (1979) Proton magnetic resonance studies of 5,6-saturated thymidine derivatives produced by ionizing radiation. Conformational analysis of 6-hydroxylated diastereoisomers. *Biochim. Biophys. Acta* **563**, 206−215.

(36) Kao, J. I., Goljer, I., Phan, T. A., and Bolton, P. H. (1993) Characterizations of the effects of a thymine glycol residue on the structure, dynamics, and stability of duplex DNA by NMR. *J. Biol. Chem.* **268**, 17787−17793.

(37) Hruska, F. E., Sebastian, R., Grand, A., Voituriez, L., and Cadet, J. (1987) Characterization of a γ-radiation-induced decomposition product of thymidine. Crystal and molecular structure of the (−) *cis* (5*R*,6*S*) thymidine glycol. *Can. J. Chem.* **65**, 2618−2623.

(38) Flippen, J. L. (1973) The crystal and molecular structures of reaction products from γ-irradiation of thyline and cytosine: *cis*-thymine glycol, C5H8N2O4, and *trans*-1-carbamoyl-imidazolidone-4,5-diol, C4H7N3O4. *Acta Crystallogr.* **B29**, 1756−1762.

(39) Miaskiewicz, K., Miller, J., and Osman, R. (1993) *Ab initio* theoretical study of the structures of thymine glycol and dihydrothymine. *Int. J. Radiat. Biol.* **63**, 677−686.

(40) Baudisch, O., and Davidson, D. (1925) The mechanism of oxidation of thymine. 4,5-Dihydroxyhydrothymine (thymine glycol). *J. Biol. Chem.* **64**, 233−239.

(41) Cadet, J., and Téoule, R. (1973) Isomérisation des 5-bromo-5,6-dihydro-6-hydroxythymidines. Préparation des formes anomères de la thymidine et de la 1-(2-désoxy-D-érythro-pentofuranosyl)-thymine (Isomerization of 5-bromo-5,6-dihydro-6-hydroxy-thymidines. Preparation of anomeric forms of thymidine and 1-(2-deoxy-D-erythro-pentofuranosyl)thymine). *Carbohydr. Res.* **29**, 345−361.

(42) Lustig, M. J, Cadet, J., Boorstein, J., and Teebor, G. W. (1992) Synthesis of the diastereoisomers of thymidine glycol, determination of concentrations and rates of interconversion of their *cis*−*trans* epimers at equilibrium and demonstration of differential alkali lability within DNA. *Nucleic Acids Res.* **20**, 4839−4845.

(43) Declercq, J. P., Germain, G., Main, P., and Woolfson, M. M. (1973) On the application of phase relationship to complex structures. V. Finding the solution. *Acta Crystallogr.* **A29**, 231−234.

(44) Busing, W. R., Martin, K. O., and Levy, H. A. (1971) ORFLS3, Report ORNL 59-4-37. Oak Ridge National Laboratory, Oak Ridge, TN.

(45) Cremer, D., and Pople, J. A. (1975) A general definition of ring puckering coordinates. *J. Am. Chem. Soc.* **97**, 1354−1358.

(46) Khon, W., and Sham, L. J. (1965) Self-consistent equations including exchange and correlation effects. *Phys. Rev.* **A140**, 1133−1138.

(47) Vosko, S. H., Wilk, L., and Nusair, M. (1980) Accurate spin-dependent electron liquid correlation energies for local spin density calulation: a critical analysis. *Can. J. Phys.* **58**, 1200−1211.

(48) Sambe, H., and Felton, R. H. (1975) A new computational approach of the Slater's Xα equation. *J. Chem. Phys.* **62**, 1122−1126.

(49) Dunlap, B. I., Connolly, J. W. D., and Sabin, J. R. (1979) On some approximations in applications of Xα theory. *J. Chem. Phys.* **71**, 3396−3402.

(50) UNICHEM2.3 (1994) Cray Research Inc., 2360 Pilot Knob Rd., Mendota Heights, MN 55120.

(51) Andzelm, J., Radzio, E., and Salahub, D. R. (1985) Compact basis sets for LCAO-LSD calculations. Part I. Method and bases for scandium to zinc. *J. Comput. Chem.* **6**, 520−532.

(52) Godbout, N., Salahub, D. R., Andzelm, J., and Wimmer, E. (1992) Optimization of gaussian-type basis sets for local spin density functionnal calculations. Part I. Boron through neon, optimization technique and validation. *Can. J. Chem.* **70**, 560−571.

(53) Becke, A. D. (1988) Density functionnal exchange-energy approximation with correct asymptotic behaviour. *Phys. Rev.* **A38**, 3098−3100.

(54) Becke, A. D. (1988) A multicenter numerical integration scheme for polyatomic molecules. *J. Chem. Phys.* **88**, 2547−2552.

(55) Perdew, J. P. (1986) Density functionnal approximation for the correlation energy of the inhomogeneous electron gas. *Phys. Rev.* **B33**, 8822−8824.

(56) Schlegel, H. B. (1987) *Ab initio Methods in Quantum Chemistry* (Lawley, K. P., Ed.) p 249, Wiley.

(57) Mulliken, R. S. (1955) Electronic population analysis on LCAO-MO molecular wave functions. *J. Chem. Phys.* **23**, 1833−1840.

(58) Grand, A., and Cadet, J. (1978) Crystal and molecular structure of (−)-(5*S*)-5-hydroxy-5,6-dihydrothymidine. *Acta Crystallogr.* **B34**, 1524−1528.

(59) Altona, C., and Sundaraligam, M. (1972) Conformational analysis of the sugar ring in nucleosides and nucleotides. A new description using the concept of pseudorotation. *J. Am. Chem. Soc.* **94**, 8205−8212.

(60) Saenger, W. (1983) *Principles of nucleic acid structure*, Chapters 2 and 4, Springer Verlag, New York.

(61) Frisch, M. J., Trucks, G. W., Head-Gordon, M., Gill, P. M. W., Wong, M. W., Foresman, J. B., Johnson, B. G., Schlegel, H. B., Robb, M. A., Replogle, E. S., Gomperts, R., Andres, J. L., Raghavachari, K., Binkley, J. S., Gonzales, C., Martin, R. L., Fox, D. J., DeFrees, D. J., Baker, J., Stewart, J. J. P., and Pople, J. A. (1992) GAUSSIAN92. Gaussian Inc., Pittsburgh, PA.

TX9501344